Civil Engineering Infrastructures Journal 2023, 56(2): 235-255
DOI: 10.22059/CEIJ.2023.342419.1837

RESEARCH PAPER

A Simplified Continuum Damage Model for Nonlinear Seismic Analysis of Concrete Arch Dams Using Different Damping Algorithms

Hashempour, S.A.R.[1], Akbari, R.[1*] and Lotfi, V.[2]

[1] M.Sc., Department of Civil and Environmental Engineering, Amirkabir University of Technology (Tehran Polytechnic), Tehran, Iran.
[2] Professor, Department of Civil and Environmental Engineering, Amirkabir University of Technology (Tehran Polytechnic), Tehran, Iran.

Received: 02 May 2022; Revised: 14 Sep 2022; Accepted: 22 Oct. 2022

ABSTRACT: In this research, a nonlinear model is presented to explore the seismic response of concrete arch dams. This model is much more simplified and efficient in comparison with plastic-damage models. It can represent softening, hardening and stiffness degradation of concrete due to load reversal. Additionally, it is able to predict the final and residual strength of the structure in softening with good accuracy. Employing different scale factors to monitor the failure of the dam, this model is used to analyze the nonlinear response of Morrow Point arch dam. The dam-reservoir interaction is considered with modified Westergaard's approach, and the dam body is modeled with second order 20-node isoparametric elements. Moreover, two different damping algorithms are included to evaluate their impact on nonlinear analysis. It is concluded that the employed model can predict realistic crack patterns through the dam body, and it can be a good replacement for other time consuming and complicated models. In addition, it is shown that the damping algorithm plays a significant role in the nonlinear dynamic analysis of concrete arch dams.

Keywords: Concrete Arch Dams, Damage Mechanics, Different Damping Algorithms, Finite Element, Nonlinear Model.

1. Introduction

Most of the concrete dams have been built based on simple and inadequate seismic design assumptions in the past. Therefore, the seismic safety of these essential infrastructures needed for water supply and flood control is upon question. Moreover, the endangered population in downstream of dams is expanding continuously. Therefore, the failure of dams would lead to drastic socioeconomic damages. The increasing concern of the seismic safety of such critical structures has created a high demand for nonlinear models capable of reassessing existing dams.

In this regard, there are two primary nonlinear models, continuum and discrete (Jenabidehkordi, 2019; Mauludin and Oucif, 2020). In discrete models, the split between element edges is adopted, which has two major disadvantages (Cabral et al., 2019; Nguyen et al., 2019; Sinaie et al., 2018). First, connectivity should change as

* Corresponding author E-mail: r.akbari96@aut.ac.ir

crack propagates, which conflicts with the intrinsic trend of Finite Element Analysis (FEA). Second, the crack line is predetermined, and it has a fixed direction during the analysis (Qin et al., 2021; Rots and Blaauwendraad, 1989). Continuum models overcome these two significant shortcomings. They are classified into smeared crack and damage models (Ghrib and Tinawi, 1995; Park et al., 2021; Voyiadjis et al., 2021). Although researchers have employed both nonlinear approaches for the dynamic analysis of concrete arch dams (Alegre et al., 2022; Alegre and Oliveira, 2020; Ardakanian et al., 2006; Mirzabozorg et al., 2007, 2004; Mirzabozorg and Ghaemian, 2005; Xu et al., 2017), the damage model has become more prevalent recently. The basis of the continuum damage model is using an internal variable called the damage variable to showcase the average material degradation on macro-mechanics scale (Farahani, 2005; Voyiadjis and Kattan, 2017). It should be mentioned that often plasticity theories are coupled with damage mechanics in order to consider irreversible strain that evolves during loading. In this regard, there have been researches incorporating plastic models for nonlinear analysis (Daneshyar and Ghaemian, 2019; Komasi and Beiranvand, 2021; Omidi and Lotfi, 2017a; Park et al., 2021).

There have been some researches for nonlinear analysis of concrete dams using damage-based models. Ghrib and Tinawi (1995) proposed a damage model functioning on the basic properties of fracture energy and concrete strength for exploring the nonlinear response of concrete gravity dams. Cervera et al. (1195) utilized an isotropic damage model which could consider tension and compression damage, and stiffness. A rate-dependent isotropic damage model capable of considering stiffness degradation and stiffness recovery and strain-rate sensitivity was presented by Cervera et al. (1996). Valliappan et al. (1996) investigated the seismic response of concrete gravity dams using the concept of Continuum Damage Mechanics (CDM). The damage criterion utilized in their research was a second order tensor model based on elastic-brittle characterization. The results indicated that there is a considerable difference between the seismic response of a damaged and undamaged concrete. Lee and Fenves (1998) proposed a new nonlinear model based on plastic-damage concept and investigated the seismic behavior of Koyna gravity dam. This model could consider the effect of strain softening, elastic stiffness degradation, large cracks formation and the stiffness recovery after closure of cracks. Valliappan et al. (1999) developed a finite element program based on HHT and used the nonlinear concept of CDM to present the seismic damage response of arch dams. The methodology employed was proved to be computationally efficient and consistent in its treatment of both growth and propagation of damage. In another research, Omidi and Lotfi (2017a) used a plastic-damage model in combination with the discrete crack (DC) model for 3-D cases to study the seismic damage response of concrete arch dams. The core of their material constitutive law relied on the presented model by Lee and Fenves (1998). It was proved that using the combination of DC and PD models yields a more consistent and reliable response compared to employing DC or PD approaches alone. Daneshyar and Ghaemian (2019) used a rate-dependent anisotropic PD model for dynamic analysis of concrete arch dams. In addition to material inelasticity, the nonlinearity of joints was also considered.

In a previous study by Akbari and Lotfi (2022), a simplified isotropic damage model was utilized for seismic assessment of a concrete gravity dam. In addition to its simple formulation and easy programming, it could successfully determine acceptable crack patterns in comparison to previous studies. This model was implemented in studying the nonlinear behavior of the Koyna dam utilizing three different damping algorithms. The results indicated

that the chosen damping could significantly influence the nonlinear results. Herein, the model is utilized to analyze the nonlinear behavior of concrete arch dams. This model has two internal damage variables for tensile and compressive state, separately. It also includes stiffness recovery due to load reversal as moving from tension to compression regime. The central part of the model employs Lubliner et al. (1989) stress functions to define tensile and compressive uniaxial behavior. The strain equivalence assumption is the basis of the model. The criteria for damage evolution are relatively simple and efficient which is based on two threshold effective principal stresses. This model is validated by uniaxial tension, compression, and full cyclic tension-compression tests in the initial stages. Thereafter, nonlinear response of the Koyna gravity dam is evaluated in 3-D modeling, and finally the developed program is employed for the seismic damage evaluation of Morrow Point arch dam using two different damping algorithms.

The remaining part of this paper is structured as follows. In Section 2, the fundamental equations of damage constitutive law are discussed. In Section 3, the dynamic equations of model are presented. In Section 4, three elementary clarification tests and applications of the model in 3-D analysis of Koyna dam are shown to verify the implementation of the presented model accuracy. Finally, in Section 5, by utilizing the damage model, the seismic damage response of a typical arch dam by means of three different damping algorithms is discussed.

2. Damage Constitutive Law

The stress $\boldsymbol{\sigma}$, and the effective stress $\bar{\boldsymbol{\sigma}}$ may be defined as:

$$\boldsymbol{\sigma} = (1 - D)\bar{\boldsymbol{\sigma}} \quad (1)$$

$$\bar{\boldsymbol{\sigma}} = \boldsymbol{E_0}\boldsymbol{\varepsilon} \quad (2)$$

where D, $\boldsymbol{E_0}$ and $\boldsymbol{\varepsilon}$: are damage variable, undamaged elastic rigidity matrix and strain matrix, respectively. In the present model to detect the damage in tension and compression two internal variables D^+ and D^- are considered, respectively, as the behavior of concrete in tension and compression is quite different (Cervera et al., 2017). Therefore, the Eq. (1) is changed into the following equation (Cervera and Tesei, 2017):

$$\boldsymbol{\sigma} = (1 - D^+)\bar{\boldsymbol{\sigma}}^+ + (1 - D^-)\bar{\boldsymbol{\sigma}}^- \quad (3)$$

In the presented equations the tension and compression are illustrated with (+) and (-), respectively. Damage variable D can be in the range of 0 to 1 (i.e., 0 for no damage and 1 for full damage). The D^+ and D^- are defined as follows for the present isotropic damage model:

$$D^+ = 1 - \frac{f^+_{max}}{\bar{f}^+_{max}} \quad (4)$$

$$D^- = 1 - \frac{f^-_{max}}{\bar{f}^-_{max}} \quad (5)$$

where $\bar{f}^+_{max}$and $\bar{f}^-_{max}$: are maximum tensile and compressive principal effective stresses reached up to that point in time, respectively. Moreover, f^+_{max} and f^-_{max}: are corresponding nominal uniaxial tensile and compressive stresses.

The uniaxial stress functions of Lubliner et al. (1989) are the basis of the model, which are demonstrated as follows:

$$f^+ = f_0^+\left[(1 + A^+)e^{-B^+(\varepsilon^+ - \varepsilon_0^+)} - A^+ e^{-2B^+(\varepsilon^+ - \varepsilon_0^+)}\right] \quad (6)$$

$$f^- = f_0^-\left[(1 + A^-)e^{-B^-(\varepsilon^- - \varepsilon_0^-)} - A^- e^{-2B^-(\varepsilon^- - \varepsilon_0^-)}\right] \quad (7)$$

The uni-axial stress curves of this model are illustrated in Figure 1. In the above equation, $f_0^{\pm}$: is the elastic strength of concrete, $\varepsilon^{\pm}$: is the strain and $\varepsilon_0^{\pm}$: is the maximum linear elastic strain.

The A^+ parameter can be calculated by taking the derivative of Eq. (6) at the onset of nonlinearity (i.e., $\varepsilon^+ = \varepsilon_0^+$), and setting

that equal to zero (i.e., $\frac{df^+}{d\varepsilon^+}\Big|_{\varepsilon^+=\varepsilon_0^+} = 0$) which results in:

$$A^+ = 1 \tag{8}$$

The A^- parameter can be calculated by taking the derivative of Eq. (7) at the strain corresponding to maximum compressive stress of concrete and setting that equal to zero $\left(\frac{df^-}{d\varepsilon^-}\Big|_{\varepsilon^-=\varepsilon_{max}^-} = 0\right)$. Thereafter, set the maximum compressive stress equal to f_1^-. This would lead to the following relation by defining $\beta^- = \frac{f_1^-}{f_0^-}$:

$$A^- = (2\beta^- - 1) + 2\sqrt{\beta^-(\beta^- - 1)} \tag{9}$$

In order to calculate the parameter $B^\pm$, there is a need to use specific fracture energy per characteristic length ($g = \int_0^\infty \sigma d\varepsilon^*; \varepsilon^* = \varepsilon - \varepsilon_0$), knowing the fact that this energy is equal to the area of stress-strain curve. The $B^\pm$ parameter are defined as follow:

$$B^\pm = \frac{2 + A^\pm}{\varepsilon_0^\pm \left(\frac{2EG_f^\pm}{l^{*\pm}\left(f_0^\pm\right)^2} - 1\right)} \tag{10}$$

where $G_f^\pm$ and $l^{*\pm}$: are the fracture energy and the characteristic length, respectively. $l^{*\pm}$ is derived by calculating the cube root of the tributary volume at each integration point of finite element (Oliver, 1989).

The process of calculating stress based on the CDM and updating the damage variable is depicted in Figure 2.

3. Nonlinear Dynamic Formulation

In order to solve the dynamic equilibrium equation in the time domain, a step-by-step procedure is employed (Eq. (11)).

$$\boldsymbol{M\ddot{U}} + \boldsymbol{P}\left(\boldsymbol{U}, \boldsymbol{\dot{U}}\right) = \boldsymbol{R}^{st} - \boldsymbol{MJa}_g \tag{11}$$

where $\boldsymbol{M}$: is the mass matrix, including the mass of dam body and added mass; $\boldsymbol{U}$, $\boldsymbol{\dot{U}}$ and $\boldsymbol{\ddot{U}}$: are displacement, velocity and acceleration vectors, respectively; $\boldsymbol{P}$: is the restoring force vector; $\boldsymbol{R}^{st}$: is the applied static loads, including hydrostatic pressures and gravity effects; $\boldsymbol{J}$: is the influence matrix for $\boldsymbol{a}_g$. The restoring force vector containing internal and damping forces, is defined as:

$$\boldsymbol{P}^e = \boldsymbol{F}^e + \boldsymbol{C}^e\boldsymbol{\dot{U}}^e \tag{12}$$

where $\boldsymbol{F}^e$: is the internal force vector, and in an element domain Ω_e, can be calculated as follows:

$$\boldsymbol{F}^e = \int_{\Omega_e} \boldsymbol{B}^T\boldsymbol{\sigma}d\Omega \tag{13}$$

where $\boldsymbol{B}$: is the strain-displacement transformation matrix.

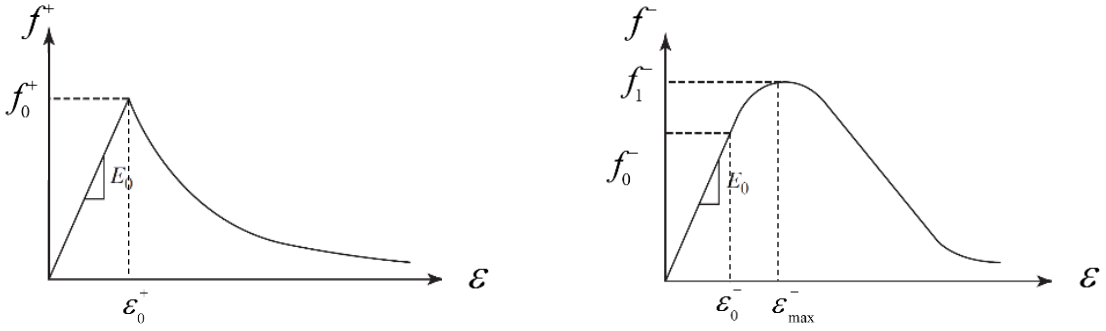

(a) Tension **(b) Compression**

Fig. 1. The uniaxial behavior of Lubliner model (Lubliner et al., 1989)

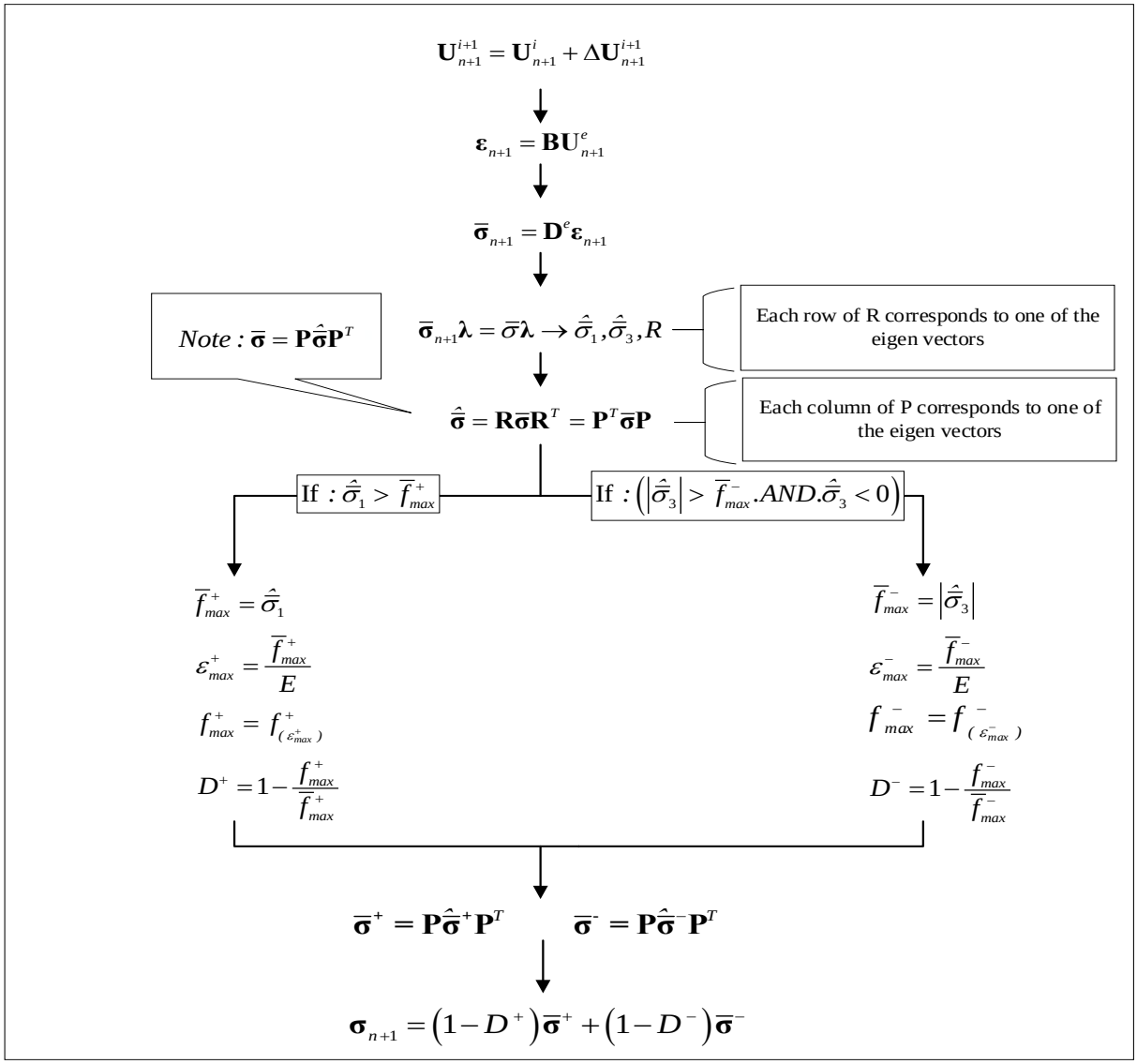

Fig. 2. The stress calculation layout with the presented model

Furthermore, $\boldsymbol{C}^{e}$: the Rayleigh damping matrix consists of damping associated with stiffness ($\boldsymbol{C}_K^e = \alpha_K \boldsymbol{K}^e$) and mass ($\boldsymbol{C}_M^e = \alpha_M \boldsymbol{M}^e$) is defined as follows (Rayleigh and Lindsay, 1945):

$$\boldsymbol{C}^{e} = \boldsymbol{C}_K^e + \boldsymbol{C}_M^e \tag{14}$$

3.1. Damping Algorithm

In this research, two different damping algorithms are utilized in dynamic equations, which are categorized based on the update time of the damping matrix in the procedure of dynamic equations and identified by JDAMP parameter. In the dynamic analysis, $\boldsymbol{C}^{e}$ is defined as:

$$\boldsymbol{C}^{\boldsymbol{e}} = \alpha_k \int_V \boldsymbol{B}^T (1 - D)\boldsymbol{E}_0 \boldsymbol{B} dV \tag{15}$$

where total damage (D), following the definition proposed by Lee and Fenves (1998), is defined as:

$$D = 1 - (1 - sD^{+})(1 - D^{-}) \tag{16}$$

The s parameter varies from 0 to 1 demonstrates stiffness recovery during the unloading process from tensile to compressive state, and can be obtained as (Lee and Fenves, 1998; Omidi and Lotfi, 2017a):

$$s = \frac{\sum_{i=1}^{3}\langle\hat{\bar{\sigma}}_i\rangle}{\sum_{i=1}^{3}|\hat{\bar{\sigma}}_i|} \tag{17}$$

The notation $\langle . \rangle$: is the Macaulay bracket, which yields the enclosed entity and zero for positive and negative values, respectively. The $\widehat{\boldsymbol{\sigma}}$: is effective principal stress matrix.

Moreover, $\boldsymbol{E}_0$: is the elastic rigidity matrix. In the first case (JDAMP = 0), the damping matrix is fixed through the whole analysis and equals to the undamaged state damping. That means:

$$\boldsymbol{C}_{n+\varphi}^{i} = \boldsymbol{C}_0 \tag{18}$$

in which $\boldsymbol{C}_0$: is explained as:

$$\begin{aligned} \boldsymbol{C}^e &= \alpha_k \int_V \boldsymbol{B}^T (1 \\ &- D)\boldsymbol{E}_0 \boldsymbol{B} dV \xrightarrow{D=0 \text{ undamaged state}} \boldsymbol{C}_0^e \\ &= \alpha_k \int_V \boldsymbol{B}^T \boldsymbol{E}_0 \boldsymbol{B} dV \end{aligned} \tag{19}$$

Therefore, the dynamic equilibrium relation can be transformed to the following equation based on the HHT method as Eq. (20). The HHT time integration method is summarized in Appendix A, which for more details can be referred to Akbari and Lotfi (2022).

$$\begin{aligned} [a_0 \boldsymbol{M} + (1-\alpha) a_1 \boldsymbol{C}_0 + (1-\alpha)\boldsymbol{K}_0] \Delta \boldsymbol{U}_{n+1}^{i+1} \\ = \boldsymbol{R}_{n+\varphi} - \boldsymbol{F}_{n+\varphi}^{i} - \boldsymbol{C}_0 \dot{\boldsymbol{U}}_{n+\varphi}^{i} \\ - \boldsymbol{M} \ddot{\boldsymbol{U}}_{n+1}^{i} \end{aligned} \tag{20}$$

In the second case (JDAMP = 1), the damping matrix would be updated just at the first iteration of each step in the analysis.

$$\boldsymbol{C}_{n+\varphi}^{i} = \boldsymbol{C}_{n+1}^{0} = \boldsymbol{C}_n \tag{21}$$

Thus, the dynamic equilibrium relation can be written as Eq. (22).

$$\begin{aligned} [a_0 \boldsymbol{M} + (1-\alpha) a_1 \boldsymbol{C}_0 + (1-\alpha)\boldsymbol{K}_0] \Delta \boldsymbol{U}_{n+1}^{i+1} \\ = \boldsymbol{R}_{n+\varphi} - \boldsymbol{F}_{n+\varphi}^{i} - C_n \dot{\boldsymbol{U}}_{n+\varphi}^{i} \\ - \boldsymbol{M} \ddot{\boldsymbol{U}}_{n+1}^{i} \end{aligned} \tag{22}$$

4. Verification of the Presented Model

To examine the accuracy of proposed model and the developed finite element program, two kinds of tests are conducted. The first one is the primary uniaxial test to investigate the capability of program for considering softening and hardening and stiffness degradation. The second test is implementation of the 3-D program for analyzing the nonlinear behavior of Koyna gravity dam to investigate the crack patterns.

4.1. Primary Test of the Model

To verify the primary behavior and accuracy of the presented nonlinear model, an eight-node three dimensional isoparametric element whose 4 nodes are constrained in the perpendicular to its plane direction and the other 4 nodes are subjected to several cyclic loadings (i.e., specified controlled displacement). Moreover, two of the adjacent side-planes are also restrained in the perpendicular directions to prevent rigid body motions in those directions. The model mechanical properties are depicted in Table 1.

The results of three different uniaxial tests are demonstrated in Figure 3. It is vivid that the model can capture softening and hardening-softening of concrete in tension and compression, respectively. Moreover, it also takes into the account the stiffness degradation regarding unloading. Furthermore, in the tension-compression test, the capability of stiffness recovery is proved when the stress state changes from tension to compression. As a result, the proposed model can determine the behavior of concrete relatively well, considering the simplicity of the model.

Table 1. Mechanical properties of the model

E(GPa)	ρ ($^{kg}/_{m^3}$)	υ	f_0^+(MPa)	f_0^-(MPa)	f_1^-(MPa)	G_f^+($^{MN}/_{m}$)	G_f^-($^{MN}/_{m}$)
30	2.580D+3	0.18	1.8	11.70	18	0.18D-3	72D-3

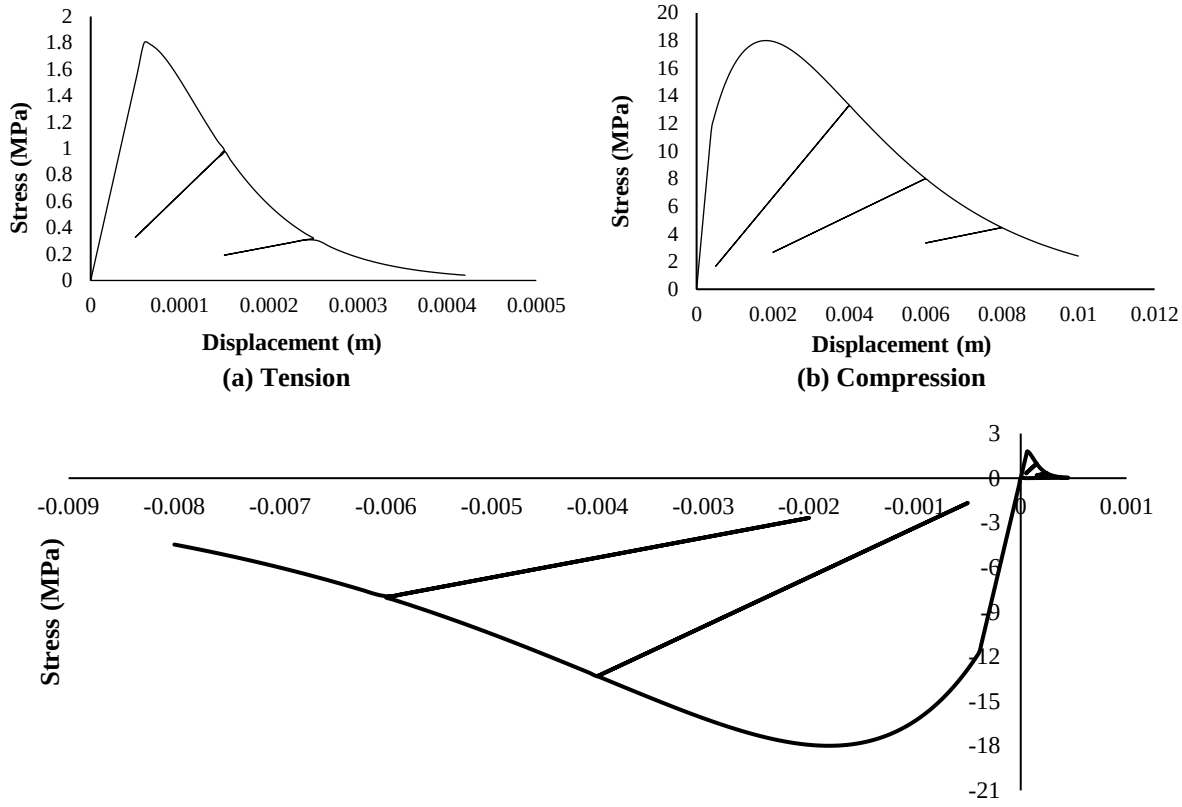

Fig. 3. Uniaxial tests on an 8-noded element

4.2. Application of the Model for Koyna Dam

Herein, the seismic response of Koyna dam with 3-dimensional 8-node elements is compared with results of the shake table test conducted in the Berkeley university laboratory (Hall, 1988). The concrete properties are: $E_0 = 30GPa$, $\rho = 2630\frac{kg}{m^3}$, $\nu = 0.2$, $f_0^+ = 2.9MPa$, $f_1^- = 24.10MPa$, $G_f^+ = 0.0002\frac{MN}{m}$ and $G_f^- = 0.02\frac{MN}{m}$. Moreover, the rigid foundation assumption and modified Westergaard method for dam-water interaction are considered (Omidi and Lotfi, 2017b). As it can be observed, the location of crack pattern in numerical results agrees with the experiment data and the accuracy of the results obtained by the personal program is quite acceptable.

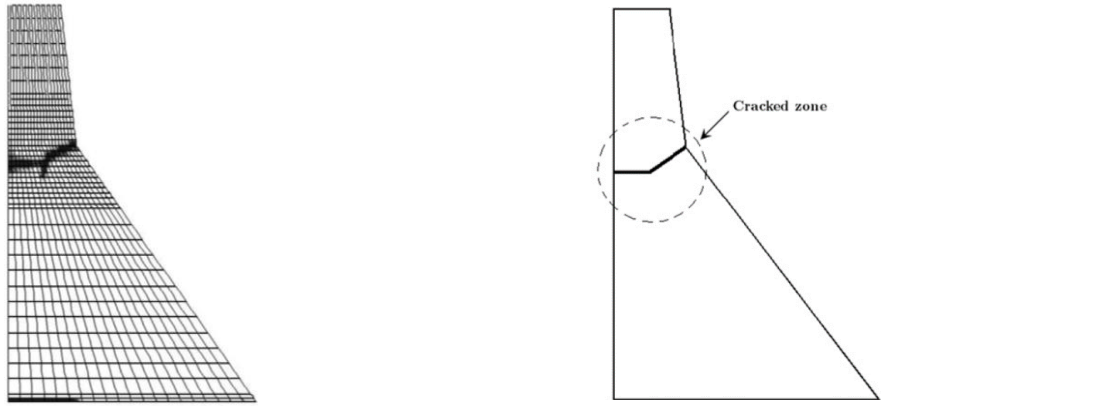

(a) Results of the presented model

(b) Experimental crack pattern at the scale of 1:150 simulation (Hall, 1988)

Fig. 4. Crack pattern of Koyna dam

5. Seismic Damage Analysis of Morrow Point Arch Dam Utilizing the Damage Model

Herein, the stability and the nonlinear behavior of Morrow Point arch dam are studied by applying the damage model previously discussed. Morrow Point is a thin-arch, double-curvature arch dam located approximately 35 km east of Montrose on the Gunnison River in southwestern Colorado. The dam structure is 143 m high with a crest length of 221 m. The thickness of the crown cantilever ranges from 3.7 m at the top to 16 m at the bottom (Wikipedia Contributors, 2022).

5.1. Numerical Simulations, Mechanical Properties and Loading

The dam is discretized by 3870 second-order isoparametric finite elements as shown in Figure 5. The hydrodynamic pressures are considered based on modified Westergaard's approach and the foundation is assumed to be rigid. These assumptions are selected to minimize computational efforts. Of course, it is vivid that the rigidity of foundation has a drastic impact on the boundary stresses in a linear analysis leading to significant tensile stresses near the base. However, these high stresses are expected to be released in the nonlinear analysis. Moreover, this release of stresses can examine the nonlinear model accuracy. The mechanical properties of concrete are depicted in Table 2.

In all analyses, time step Δt = 0.005 sec is utilized, and the stiffness coefficient of Rayleigh damping (α_k) is considered as 0.006297. The static load comprises Gravity and Hydrostatic pressures (maximum water depth = 141.73 m), and the dynamic loading is the seismic excitations consisting of the stream and the vertical components of the Taft earthquake, as demonstrated in Figure 6. The cross-canyon excitation is omitted for a complete symmetric loading condition. This can be helpful as an extra tool for the verification of the analysis results.

5.2. Analysis Results

Three analysis types are considered: a linear analysis (LN), a nonlinear analysis with damage model using constant damping option (JDAMP = 0), and a nonlinear analysis with damage model using variable damping option (JDAMP = 1). It should be mentioned that time is divided into negative and positive part. Although negative time is not real, it is just considered for static analysis, including gravity and hydrostatic loads. In this part of analysis, the gravity loads are implemented in 20 increments and the hydrostatic loads in the next 20 increments at negative range of time. The dynamic analysis started with initial conditions induced by static analysis at time zero.

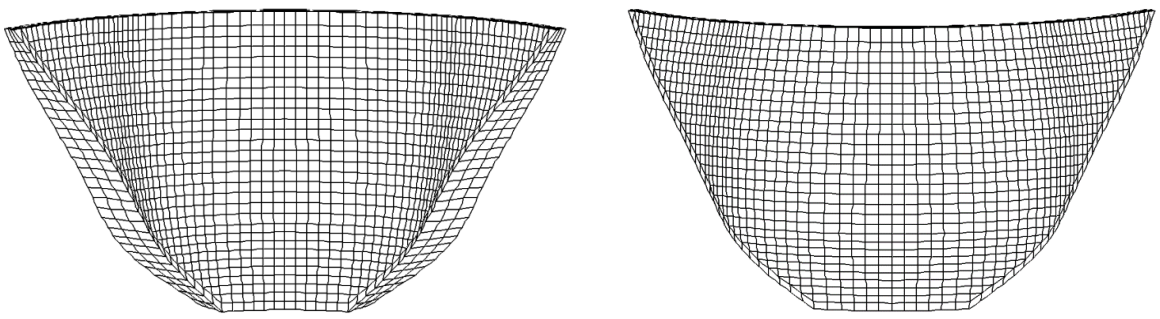

Fig. 5. Finite element mesh of Morrow Point arch dam

Table 2. Mechanical behavior of concrete

E (GPa)	ρ ($^{kg}/_{m^3}$)	υ	f_0^+(MPa)	f_0^-(MPa)	f_1^-(MPa)	$G_f^+(^{MN}/_m)$	$G_f^-(^{MN}/_m)$
27.5	2.528D+3	0.2	3.0	19.50	30.0	0.4D-3	55.0D-3

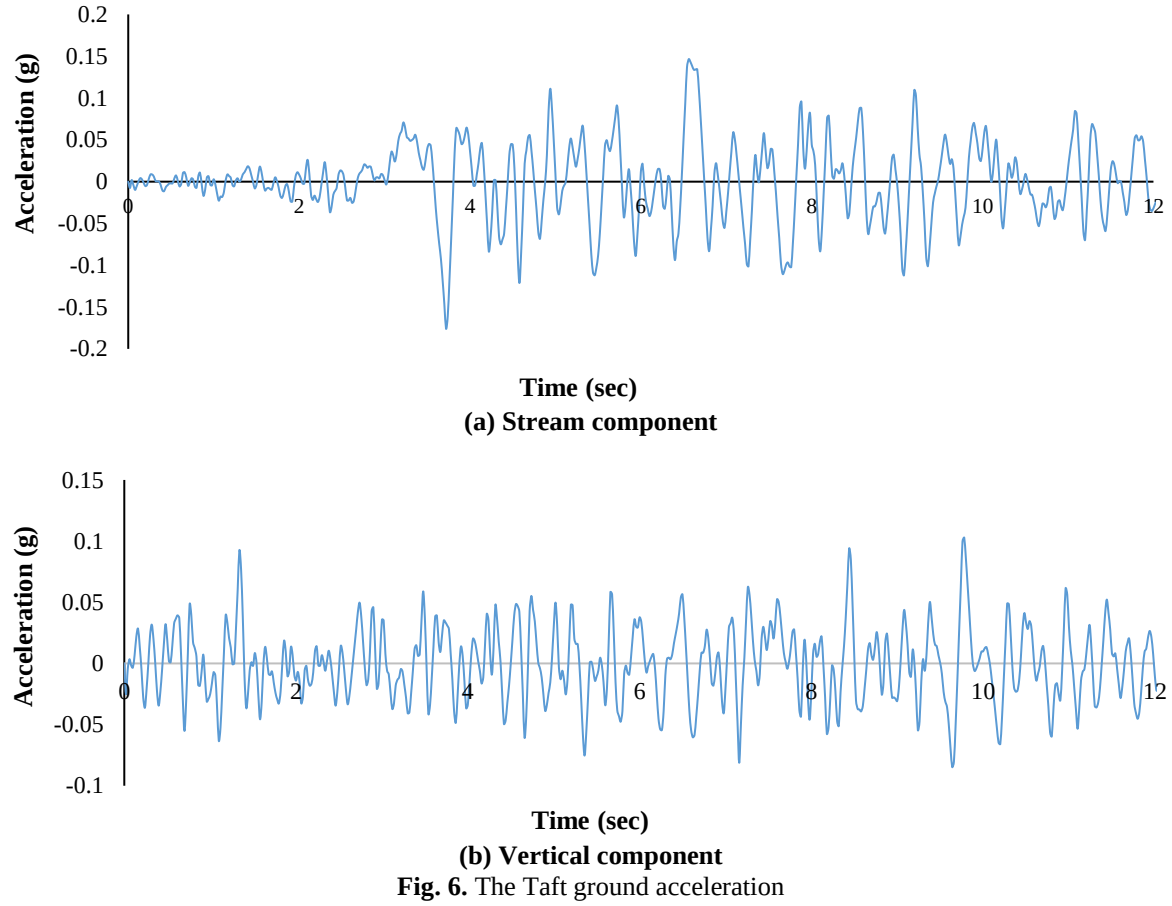

Fig. 6. The Taft ground acceleration

5.2.1. Linear Results

In this section, linear analysis results are presented. Two primary analyses are conducted for this case to examine the effect of the reservoir and various Scale Factors (SC) on the analysis results.

5.2.1.1. The Influence of Hydrodynamic Pressures

For the aim of saving computational time in this study, the exact modeling of the dam reservoir is ignored. However, an approximate method (i.e., Westergaard's approach) is used to include the effect of the hydrodynamic pressures. The time history of stream-component of dam crest displacement is depicted in Figure 7. As observed, by considering the effect of the hydrodynamic pressures, the dam crest displacement is raised significantly as expected.

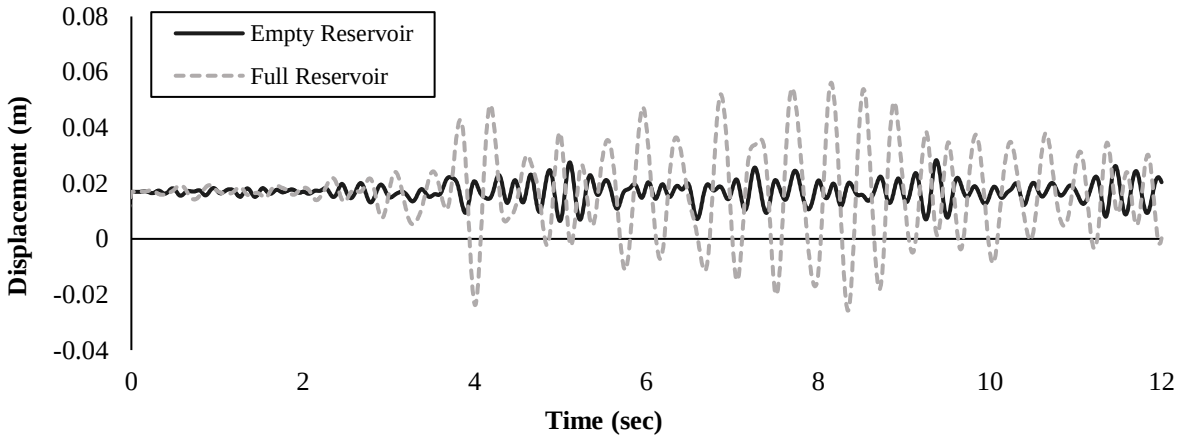

Fig. 7. The dam mid-crest displacement in the stream direction

5.2.1.2. The Effect of Different Scale Factors

To investigate the linear dynamic response of the dam under severe seismic loads, the Taft acceleration components are multiplied by a scale factor of 1.2, 1.3, and 1.4. These magnified records are applied to the dam in turn. As it can be observed, increasing the acceleration components leads to the increase in the displacement of the dam mid-crest as shown in Figure 8. Moreover, the maximum tensile principal stresses at abutments and the dam's mid-crest region are increased from 11.70 to 12.27 MPa (Figure 9). These stresses are much higher than concrete tensile strength. Therefore, these parts of the dam are presumably prone to cracks during severe earthquakes. Of course, one would actually capture much lower tensile stresses at these locations due to contraction joint or peripheral joint modeling that is neglected herein for simplification purposes. The maximum compressive principal stresses are increased from -10.61 to -11.11. Although the compressive stresses are increased, they do not surpass the concrete's compressive strength and are not a matter of concern.

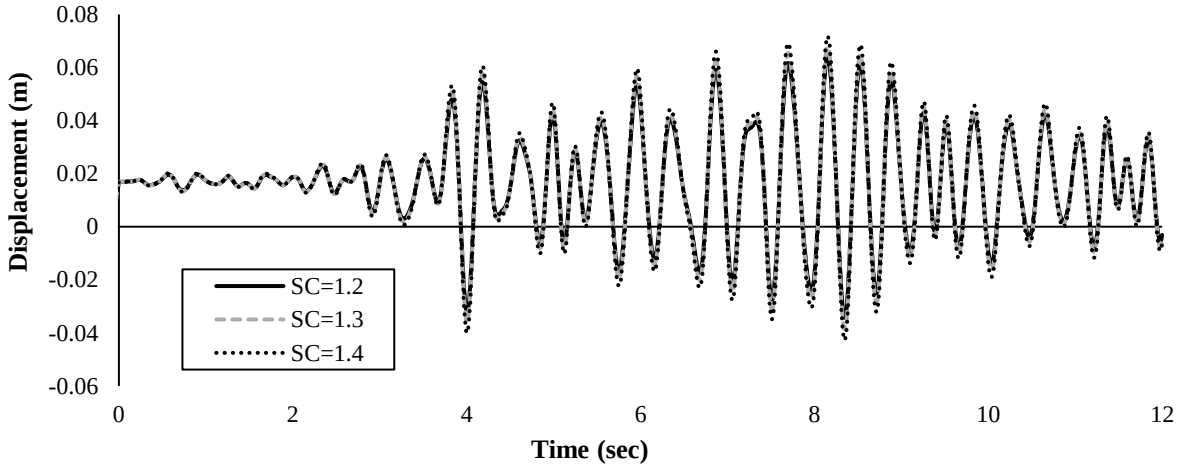

Fig. 8. The dam mid-crest displacement in the stream direction

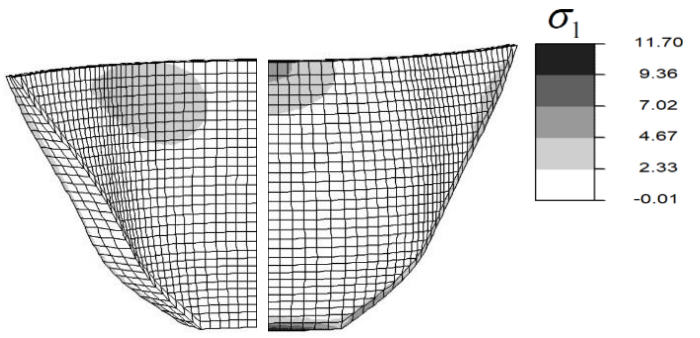

(a) Maximum tension SC = 1.2

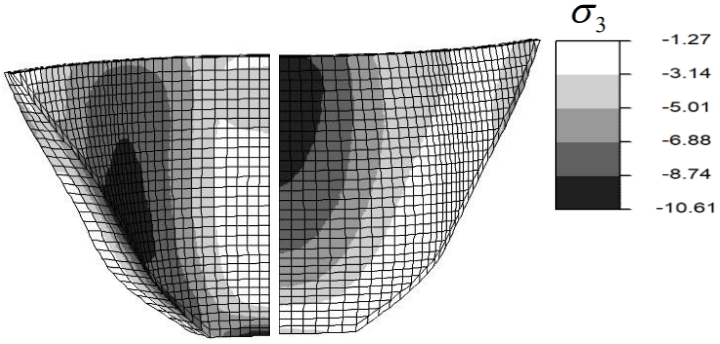

(b) Maximum compression SC = 1.2

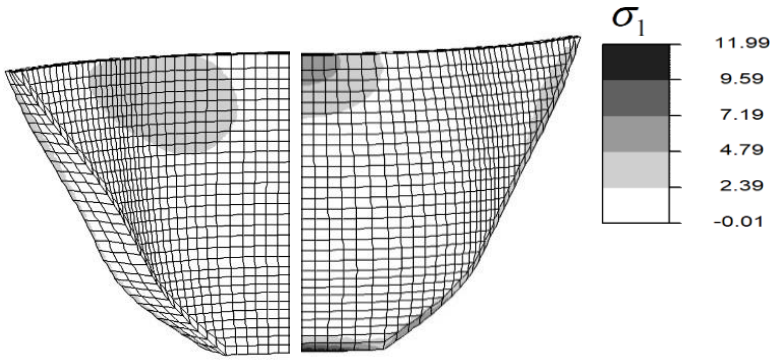

(c) Maximum tension SC = 1.3

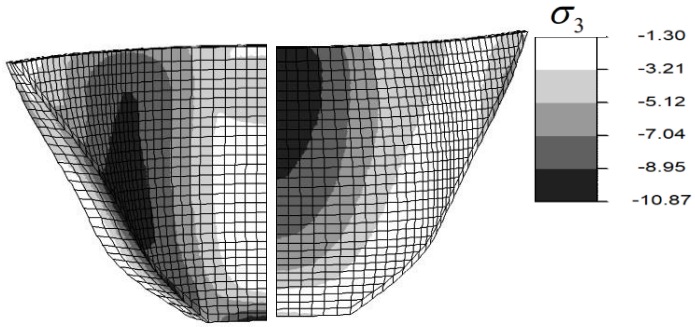

(d) Maximum compression SC = 1.3

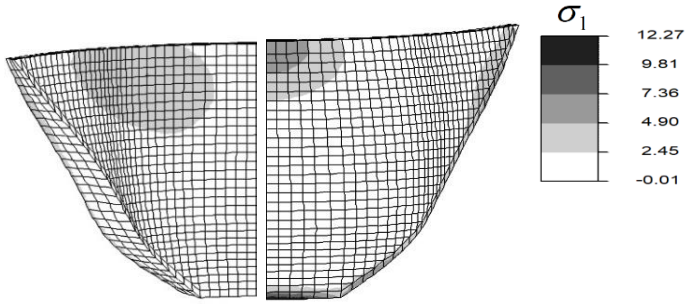

(e) Maximum tension SC = 1.4

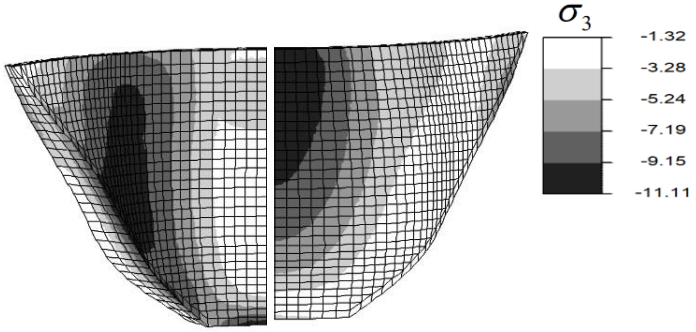

(f) Maximum compression SC = 1.4

Fig. 9. Envelope of principal stresses (MPa) for linear case

5.2.2. Nonlinear Results

In this section, two primary analyses are conducted with different damping algorithms: 1) Constant Damping (JDAMP = 0); and 2) Varying damping (JDAMP = 1). In each part, different Scale Factors (SC) of Taft acceleration are applied to the Morrow Point dam to investigate its nonlinear response due to extreme dynamic loading.

5.2.2.1. Constant Damping (JDAMP=0)

This case results are summarized in Table 3. Moreover, the envelopes of maximum tensile and compressive principal stresses throughout the analysis are

demonstrated in Figure 10. It is observed that tensile stresses are now bounded to the concrete tensile strength, illustrating one of the main capabilities of the present model. Moreover, high compressive principal stresses have occurred in the dam's mid-crest region (U/S face), dam's base and abutments (D/S face). However, they do not exceed the concrete compressive strength even for 1.4 scale factor. Therefore, no compressive damage is expected in these cases. It is also noticed that tensile and compressive stresses are distributed in a broader range as scale factor increases.

The tensile damage resulted for various parts of the dam body at the end of analysis is demonstrated in Figure 11. It is noticed that there are tensile damages in the base and abutments, as well as dam's mid-crest region on the U/S face. However, these are mainly occurring due to lack of peripheral and contraction joint modeling. Therefore, our concrete model has actually replaced joint modeling at those locations in an approximate manner. It is also noticed that there is tensile damage at dam's top portion on the D/S face which is growing in length as scale factor increases. However, it is noted that it has not yet formed a complete failure mechanism even for 1.4 scale factor.

Table 3. Maximum displacement of dam mid-crest and maximum stresses in dam body (JDAMP = 0)

Scale Factor	U_y^{Max} (mm)	U_z^{Max} (mm)	σ_1^{Max} (MPa)	σ_3^{Max} (MPa)
1.2	66.0	-4.32	3.0	-14.05
1.3	71.2	-4.33	3.0	-14.35
1.4	76.9	-4.6	3.0	-14.65

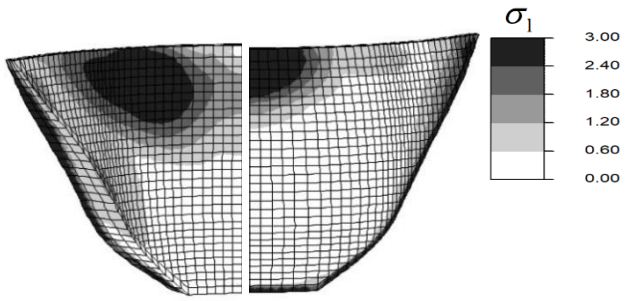

(a) Maximum tension SC = 1.2

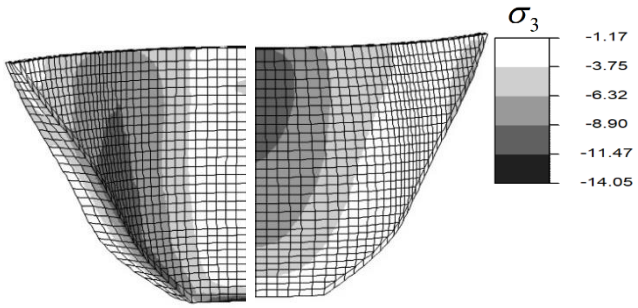

(b) Maximum compression SC = 1.2

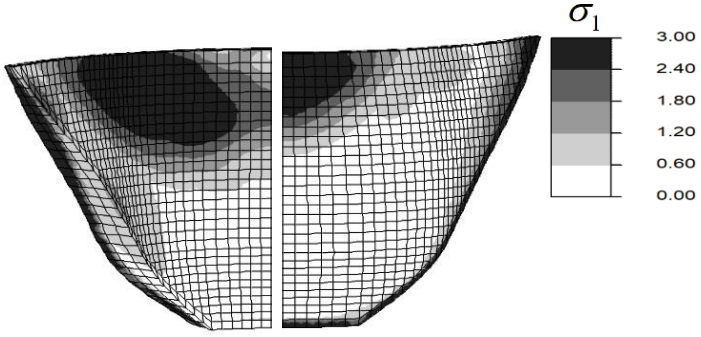

(c) Maximum tension SC = 1.3

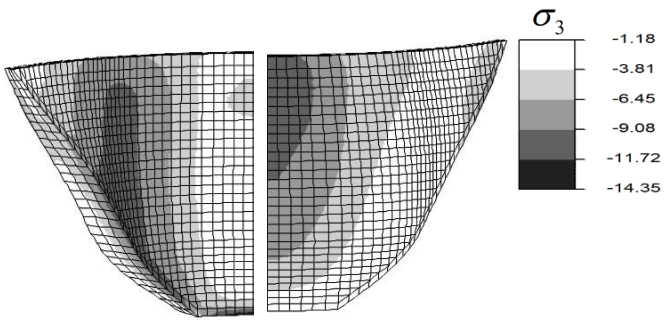

(d) Maximum compression SC = 1.3

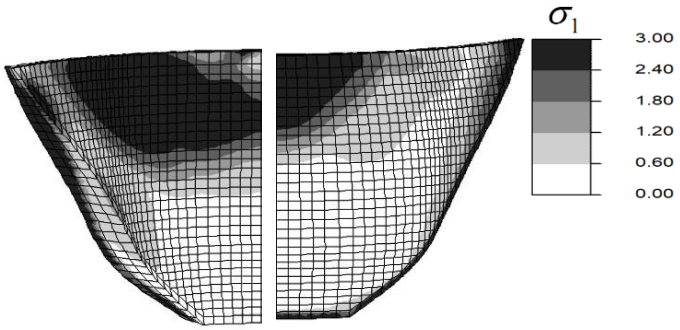

(e) Maximum tension SC = 1.4

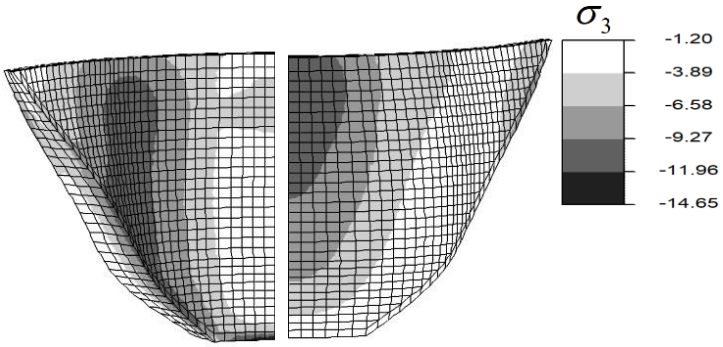

(f) Maximum compression SC = 1.4

Fig. 10. Envelope of maximum stresses nonlinear case JDAMP = 0

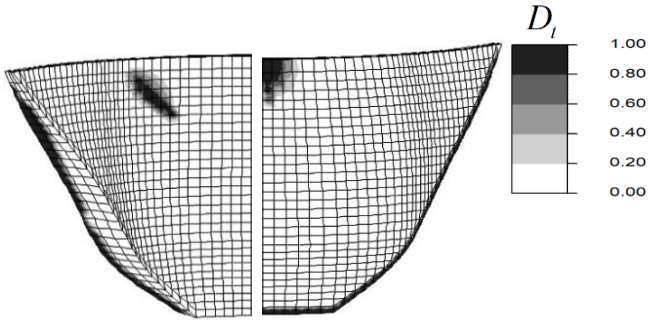

(a) SC = 1.2

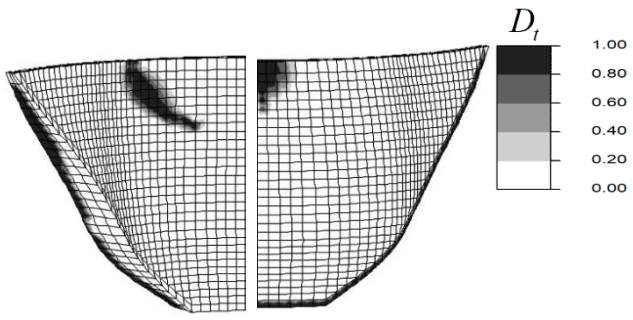

(b) SC = 1.3

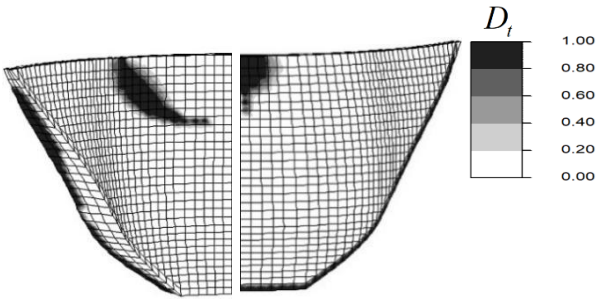

(c) SC = 1.4

Fig. 11. Distribution of damage at the end of analysis for the nonlinear case JDAMP = 0

5.2.2.2. Variable Damping (JDAMP = 1)

In this section, six models are investigated. Each model has a different scale factor. The scale factors vary from 1.2 to 1.55. These factors are increased gradually in a way that leads to the failure of the dam. The maximum dam mid-crest displacement in the stream and vertical direction are presented in Table 4. It is noticed that displacement at mid-crest increase for variable damping cases in comparison with their corresponding constant damping cases (Table 4 versus Table 3). Moreover, when the scale factor exceeds 1.4, displacement of the dam mid-crest has a considerable amount of increase which is the initial sign of failure. For 1.55 scale factor, the stream-component of displacement reaches a high value of 22 cm. Moreover, the displacement of the dam mid-crest in the stream direction in the range of 6 to 12 sec (where the notable changes have been happened) is shown in Figure 12.

The envelopes of maximum tensile and compressive principal stresses are also depicted in Figure 13. Moreover, tensile damage for these cases is presented in Figure 14. It is noticed that there is more extensive tensile damage for variable damping cases in comparison with corresponding constant damping cases. Moreover, the maximum compressive principal stresses have also increased. For instance, when we consider the 1.4 scale factor case of variable damping, it is noticed that tensile damage on the top portion form a complete loop on the D/S face while this is not the case for corresponding constant damping case. Furthermore, the maximum compressive principal stresses reach a high value of -20.99 MPa (in comparison with -14.65 MPa for corresponding constant damping case).

It is also noted that as scale factor reaches the value of 1.55, the tensile damage at the top portion extends along the dam thickness and similar loop begins to form starting at dam crest. This means that we are getting very close to a complete failure mechanism occurring at the top portion of the dam. Moreover, the maximum compressive principal stress reaches a high value of -29.96 MPa and its location is at dam mid-crest which is a sign of crushing in that vicinity.

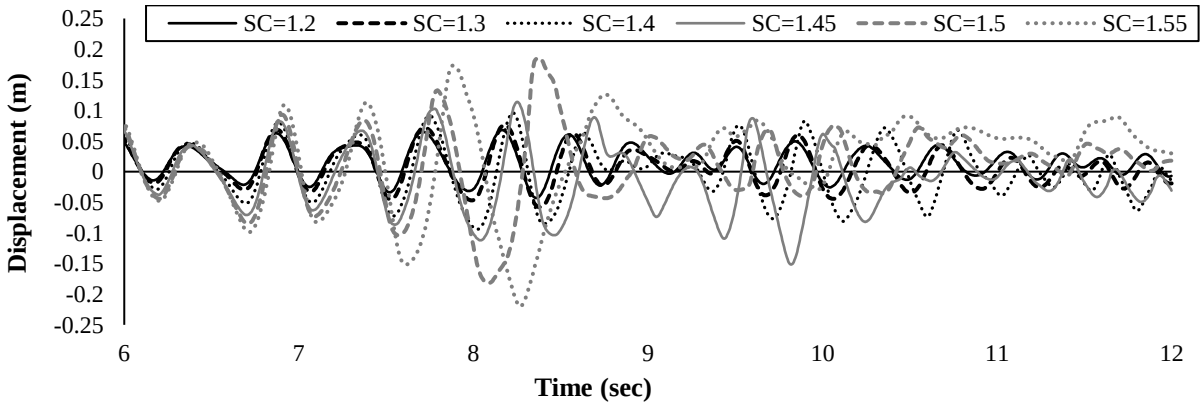

Fig. 12. The dam mid-crest displacement in the stream direction in the nonlinear case

Table 4. Maximum displacement of dam mid-crest and maximum stresses in dam body (JDAMP = 1)

Scale factor	U_y^{Max} (mm)	U_z^{Max} (mm)	σ_1^{Max} (MPa)	σ_3^{Max} (MPa)
1.2	67.9	-4.46	3.0	-14.50
1.3	76.4	-8.24	3.0	-14.77
1.4	96.4	-11.4	3.0	-20.99
1.45	-152	21.5	3.0	-26.42
1.5	186	38.0	3.0	-29.58
1.55	-220	70.9	3.0	-29.96

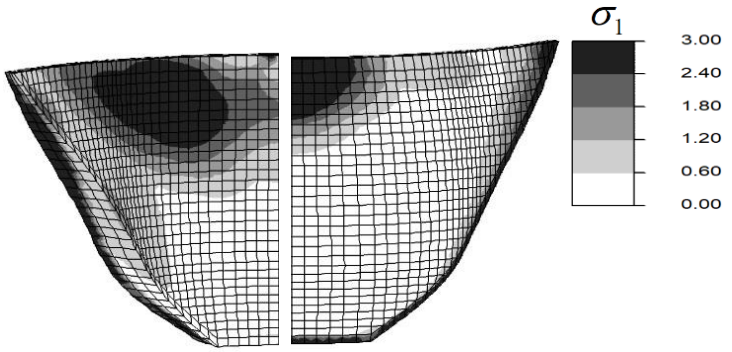

(a) Maximum tension SC = 1.2

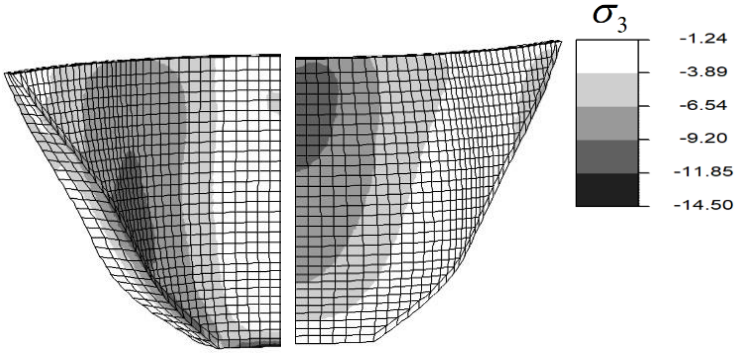

(b) Maximum compression SC = 1.2

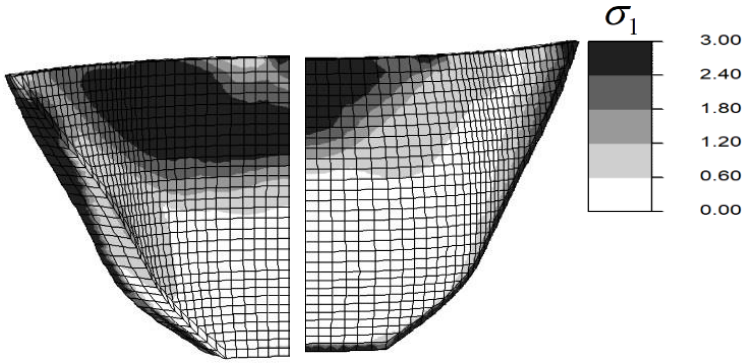

(c) Maximum tension SC = 1.3

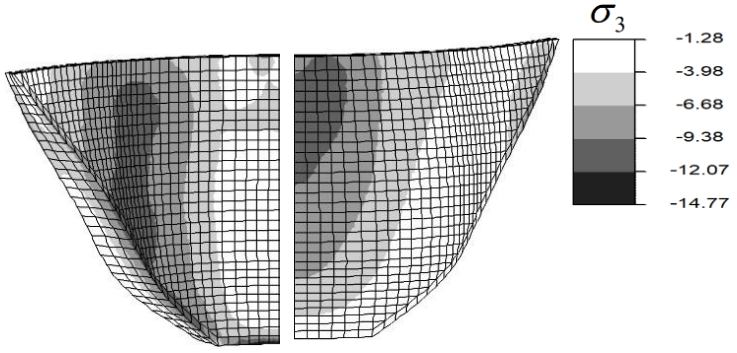

(d) Maximum compression SC = 1.3

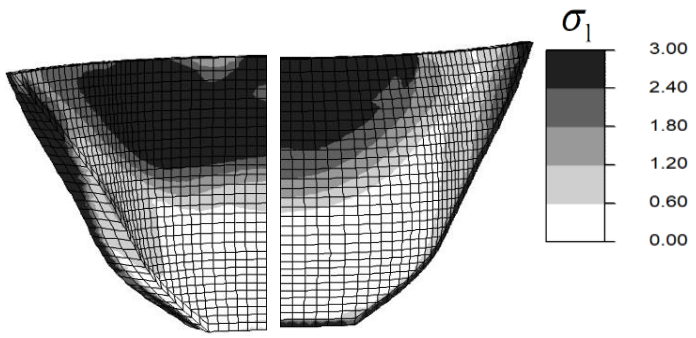

(e) Maximum tension SC = 1.4

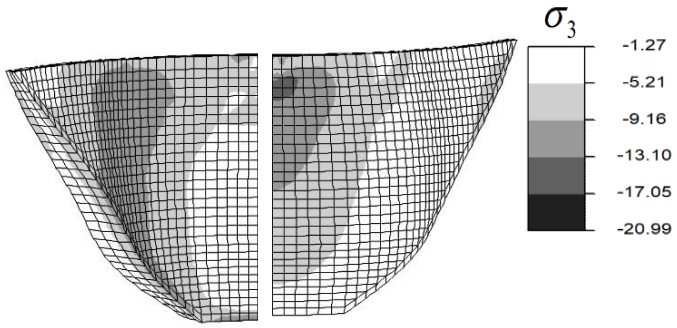

(f) Maximum compression SC = 1.4

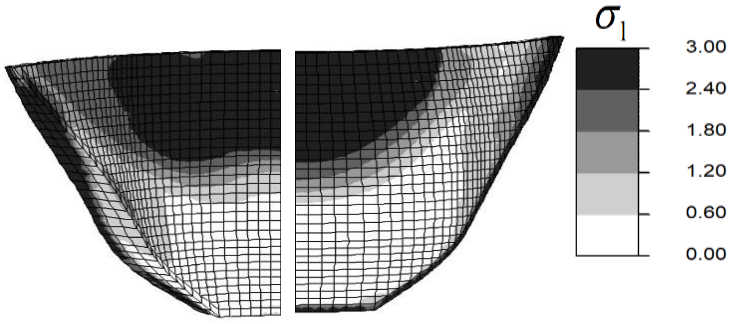

(g) Maximum tension SC = 1.45

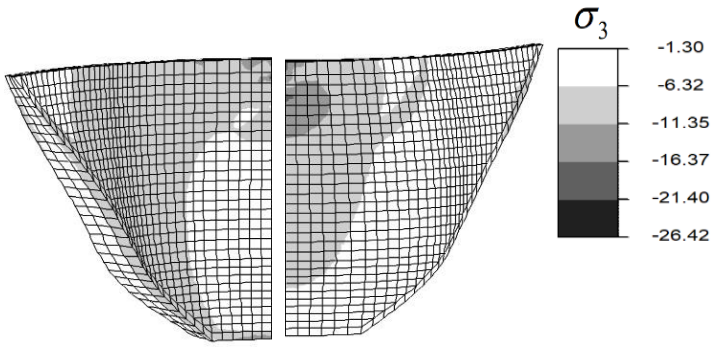

(h) Maximum compression SC = 1.45

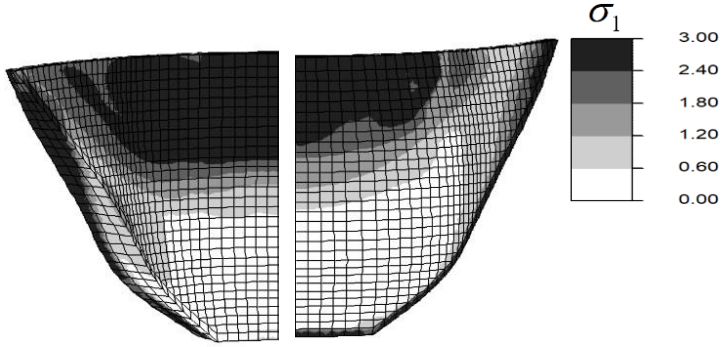

(i) Maximum tension SC = 1.5

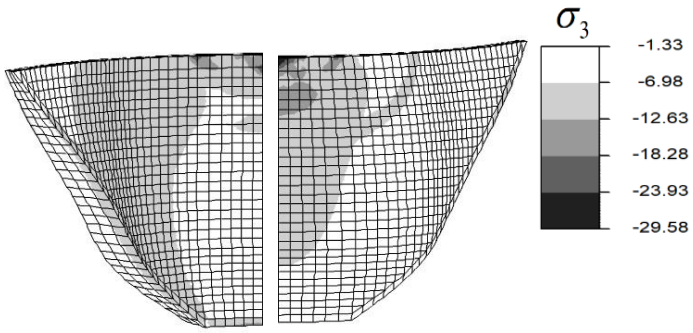

(j) Maximum compression SC = 1.5

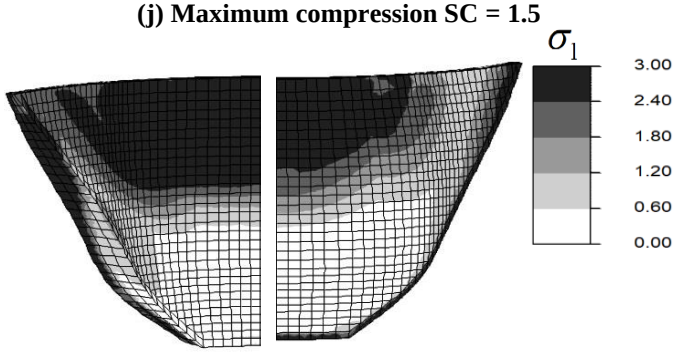

(k) Maximum tension SC = 1.55

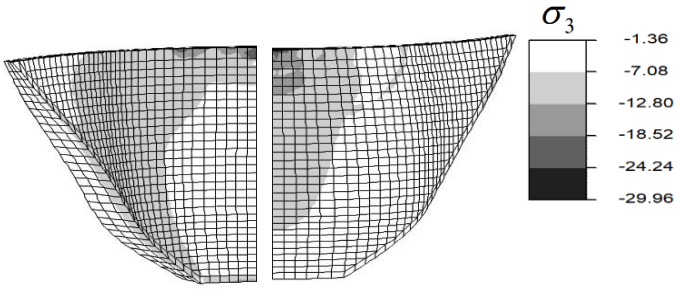

(l) Maximum compression SC = 1.55

Fig. 13. Envelope of maximum stresses in nonlinear case JDAMP = 1

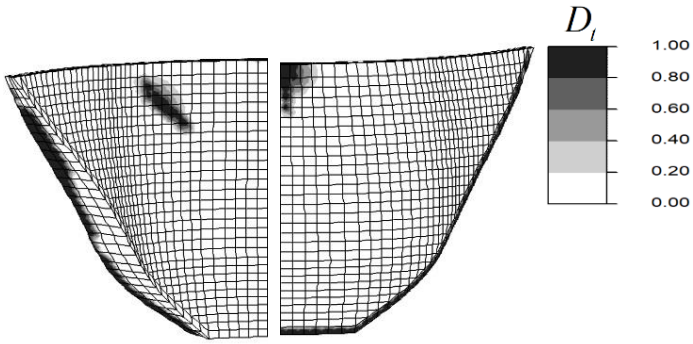

(a) SC = 1.2

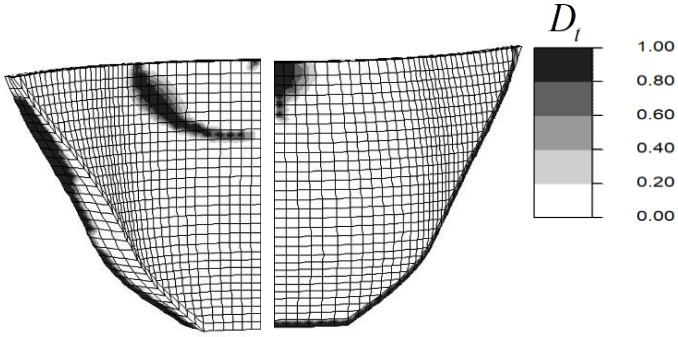

(b) SC = 1.3

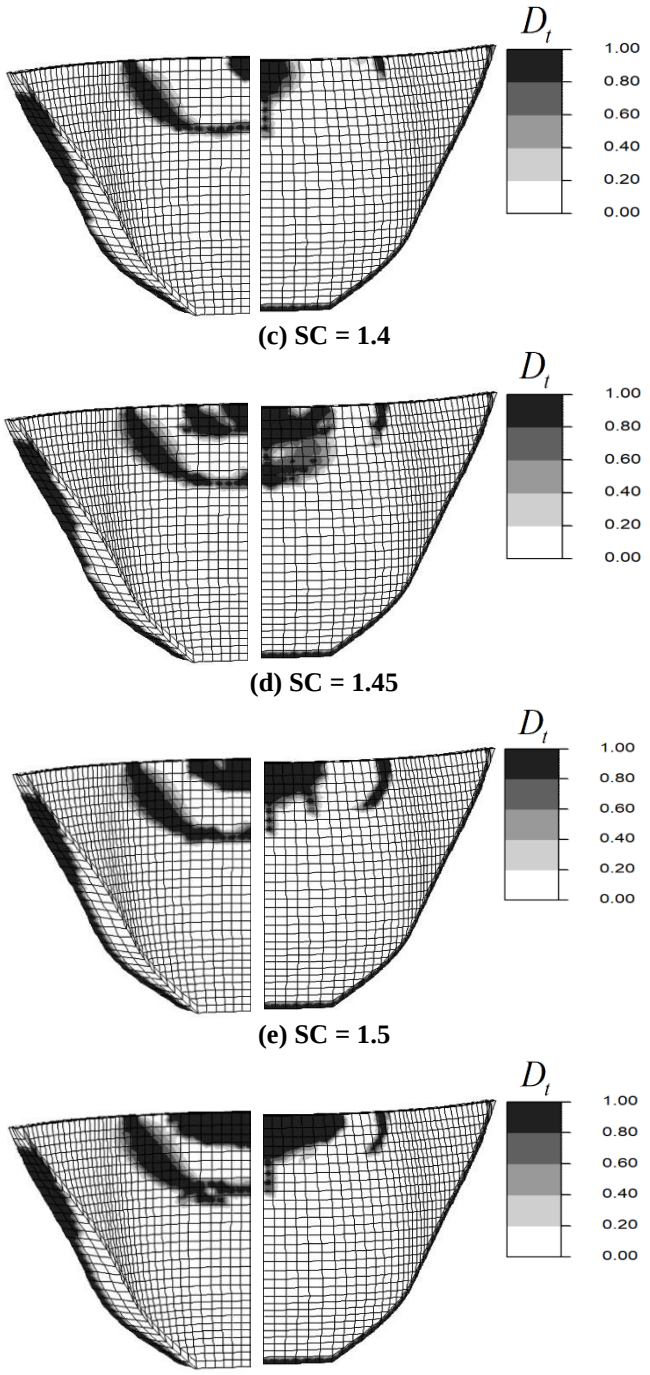

(c) SC = 1.4

(d) SC = 1.45

(e) SC = 1.5

(f) SC = 1.55

Fig. 14. Distribution of damage at the end of analysis for the nonlinear case JDAMP = 1

6. Summary and Conclusions

A special finite element program based on the proposed damage model was developed to evaluate the seismic damage response of concrete arch dams. An idealized symmetric model of 143 m high Morrow Point dam located in Colorado was subjected to Taft earthquake components. The components of the earthquake were multiplied by different scale factors to investigate the failure of the dam. Three cases were analyzed; 1) Linear case; 2) Nonlinear case with constant damping; 3) Nonlinear case with variable damping. The principal outcomes are summarized as follows:

- The proposed nonlinear model can predict the ultimate strength of the structure and the process of forming cracks in the arch dam.
- Considering the effect of the reservoir

has a significant impact on the analysis results

- Morrow Point arch dam can stand high compressive stresses; however, its tensile strength cannot bear the induced stresses, so tensile damage is inevitable, and cracks will be formed.
- The displacements and stresses are increased in the case of variable damping more than in constant damping case with the same alpha factors which is due to the update of damping matrix leading to softening of structure.
- In the case of constant damping, the main location of tensile damages is in the base and abutments, as well as dam's mid-crest region on the U/S face, and dam's top portion on the D/S face in which by increasing the scale factor, they tend to grow in length and form an unstable part on the crest of the dam.
- In the case of variable damping, the main location of tensile cracks is the same as the constant damping case. However, it seems that cracks are extended more in this case, and they form a complete loop on the D/S face of the top portion.
- The analyses indicate an early sign of failure in the structure based on the adopted methodology when significant displacements are enforced on the dam due to severe seismic loadings.
- This model can practically restrain the maximum tensile stresses to the tensile strength of concrete, and predicts a realistic distribution and stress levels in the dam body.
- The nonlinear case results with variable damping demonstrate that the arch dam can experience considerable damage in the time of a strong earthquake and when the scale factor reaches 1.55, there is the probability of failure.
- Overall, the model is proved to predict crack propagation consistent with failure in concrete arch dams. Moreover, this model is undoubtedly a step toward reducing the computational time while having an acceptable level of accuracy in dam engineering practice.

7. Appendix A

Table A.1: The HHT time integration method

0	$\boldsymbol{i=0}$, $\boldsymbol{\dot{U}^0_{n+1} = -a_4\dot{U}_n - a_5\ddot{U}_n}$, $\boldsymbol{\ddot{U}^0_{n+1} = -a_2\dot{U}_n - a_3\ddot{U}_n}$ and $\boldsymbol{U^0_{n+1} = U_n}$
1	$R_{n+1} = R^{st} - MJa^g_{n+1}$
2	$U^i_{n+\varphi} = \alpha U_n + (1-\alpha)U^i_{n+1}$
3	$\varepsilon_{n+\varphi} = B(U^e)^i_{n+\varphi}$, then obtain $\sigma_{n+\varphi}$and $D_{n+\varphi}$
4	$\Psi^i_{n+1} = M\ddot{U}^i_{n+1} + C\dot{U}^i_{n+\varphi} + F^i_{n+\varphi} - R_{n+\varphi}$
5	IF $\left\|\Psi^i_{n+1}\right\| \le Tol_G$ Then Exit
6	Solve $\left(\frac{\partial\Psi}{\partial U}\right)_{n+1} \Delta U^{i+1}_{n+1} = -\Psi^i$
7	$U^{i+1}_{n+1} = U^i_{n+1} + \Delta U^{i+1}_{n+1}$
8	$\dot{U}^{i+1}_{n+1} = \dot{U}^i_{n+1} + a_1\Delta U^{i+1}_{n+1}$
9	$U^{i+1}_{n+1} = \ddot{U}^i_{n+1} + a_0\Delta U^{i+1}_{n+1}$
10	i=i+1 and GOTO Step 2.

6. References

Akbari, R. and Lotfi, V. (2022). "Nonlinear dynamic analysis of concrete gravity dams utilizing a simplified continuum damage model and different damping algorithms", *Asian Journal of Civil Engineering*, 24(2), 453-468, https://doi.org/10.1007/s42107-022-00511-2.

Alegre, A. and Oliveira, S. (2020). "Non-linear seismic analysis of arch dams considering joint movements and a concrete damage model", *Dam World 2020*, Lisbon, Portugal.

Alegre, A., Oliveira, S., Mendes, P., Proença, J., Carvalho, E. and Matsinhe, B. (2022). "Numerical models for seismicanalysis of arch dams", *Congreso de Métodos Numéricos En Ingeniería*, 1-20.

Ardakanian, R., Ghaemian, M. and Mirzabozorg, H. (2006). "Nonlinear behavior of mass concrete in 3-D problems using damage mechanics approach", *European Earthquake Engineering*, 20(2), 65-89.

Cabral, N.R., Invaldi, M.A., D'Ambra, R.B. and Iturrioz, I. (2019). "An alternative bilinear peridynamic model to simulate the damage process in quasi-brittle materials", *Engineering Fracture Mechanics*, 216(1), 106494, DOI:10.1016/j.engfracmech.2019.106494.

Cervera, M., Oliver, J. and Faria, R. (1995). "Seismic evaluation of concrete dams via continuum damage models" *Earthquake Engineering & Structural Dynamics*, 24(9), 1225-1245, https://doi.org/10.1002/eqe.4290240905.

Cervera, M., Oliver, J. and Manzoli, O., (1996). "A rate-dependent isotropic damage model for the seismic analysis of concrete dams", *Earthquake Engineering & Structural Dynamics*, 25(9), 987–1010, 25, 987-1010,

https://doi.org/10.1002/(SICI)1096-9845(199609)25:9<987::AID-EQE599>3.0.CO;2-X.

Cervera, M. and Tesei, C. (2017). "An energy-equivalent d+/d− damage model with enhanced microcrack closure-reopening capabilities for cohesive-frictional materials", *Materials*, 10(4), 433. https://doi.org/10.3390/ma10040433.

Cervera, M., Tesei, C. and Ventura, G. (2017). "Cracking of quasi-brittle structures under monotonic and cyclic loadings: A d+/d− damage model with stiffness recovery in shear", *International Journal of Solids and Structures*, 135(1), 148-171, https://doi.org/10.1016/j.ijsolstr.2017.11.017.

Daneshyar, A. and Ghaemian, M. (2019). "Seismic analysis of arch dams using anisotropic damage-plastic model for concrete with coupled adhesive-frictional joints response", *Soil Dynamics and Earthquake Engineering* 125(1), 105735, https://doi.org/10.1016/J.SOILDYN.2019.105735.

Farahani, A.V. (2005). *Advances in fatigue, fracture and damage assessment of materials*, Vol. 6, WIT Press.

Ghrib, F. and Tinawi, R., (1995. "Nonlinear behavior of concrete dams using damage mechanics", *Journal of Engineering Mechanics*, 121(4), 513-527, https://doi.org/10.1061/(ASCE)0733-9399(1995)121:4(513).

Hall, J.F. (1988). "The dynamic and earthquake behaviour of concrete dams: review of experimental behaviour and observational evidence", *Soil Dynamics and Earthquake Engineering* 7(2), 58-121, issue?? https://doi.org/10.1016/S0267-7261(88)80001-0.

Jenabidehkordi, A. (2019). "Computational methods for fracture in rock: A review and recent advances", *Frontiers of Structural and Civil Engineering*, 13(2), 273-287.

Komasi, M. and Beiranvand, B. (2021). "Seepage and stability analysis of the Eyvashan Earth Dam under drawdown conditions", *Civil Engineering Infrastructures Journal*, 54(2), 205-223, https://doi.org/10.22059/ceij.2020.293429.1634.

Lee, J. and Fenves, G.L. (1998). "A plastic-damage concrete model for earthquake analysis of dams", *Earthquake Engineering & Structural Dynamics*, 27(9), 937-956, https://doi.org/10.1002/(SICI)1096-9845(199809)27:9<937::AID-EQE764>3.0.CO;2-5.

Lubliner, J., Oliver, J., Oller, S. and Oñate, E., (1989). "A plastic-damage model for concrete", *International Journal of Solids and Structures*, 25(3), 299-326, https://doi.org/10.1016/0020-7683(89)90050-4.

Mauludin, L.M. and Oucif, C. (2020). "Computational modeling of fracture in concrete: A review", *Frontiers of Structural and Civil Engineering*, 14(3), 586-598, https://doi.org/10.1007/s11709-020-0573-z.

Mirzabozorg, H. and Ghaemian, M. (2005). "Non-linear behavior of mass concrete in three-dimensional problems using a smeared crack approach", *Earthq Eng Struct Dyn*, 34(3), 247-269, https://doi.org/10.1002/eqe.423.

Mirzabozorg, H., Ghaemian, M. and Kianoush, M.R. (2004). "Damage mechanics approach in seismic analysis of concrete gravity dams including dam-reservoir interaction", *European Earthquake Engineering*, 18(3), 17-24.

Mirzabozorg, H., Khaloo, A.R., Ghaemian, M. and Jalalzadeh, B. (2007). "Non-uniform cracking in smeared crack approach for seismic analysis of concrete dams in 3D space", *International Journal of Earthquake Engineering and Engineering Seismology* (EEE), 2(1), 48-57.

Nguyen, N.H.T., Bui, H.H., Kodikara, J., Arooran, S. and Darve, F. (2019). "A discrete element modelling approach for fatigue damage growth in cemented materials", *International Journal of Plasticity*, 112(1), 68-88, https://doi.org/https://doi.org/10.1016/j.ijplas.2018.08.007.

Oliver, J., (1989). "A consistent characteristic length for smeared cracking models", *International Journal for Numerical Methods in Engineering*, 28(2), 461-474, https://doi.org/10.1002/nme.1620280214.

Oliver, J., Cervera, M., Oller, S. and Lubliner, J. (1990). "Isotropic damage models and smeared crack analysis of concrete", *Proceedings of SCI-C Computer Aided Analysis and Design of Concrete Structures*, Pineridge Press, pp. 945-957.

Omidi, O. and Lotfi, V. (2017a). "Seismic plastic–damage analysis of mass concrete blocks in arch dams including contraction and peripheral joints", *Soil Dynamics and Earthquake Engineering*, 95(1), 118-137, https://doi.org/10.1016/j.soildyn.2017.01.026.

Omidi, O. and Lotfi, V. (2017b). "A symmetric implementation of pressure-based fluid-structure interaction for nonlinear dynamic analysis of arch dams", *Journal of Fluids and Structures*, 69(1), 34-55, https://doi.org/https://doi.org/10.1016/j.jfluidstructs.2016.12.003.

Park, T., Ahmed, B. and Voyiadjis, G.Z., (2021). "A review of continuum damage and plasticity in concrete, Part I: Theoretical framework", *International Journal of Damage Mechanics*, 31(6), 901-954, https://doi.org/10.1177/10567895211068174.

Qin, X., Guo, J., Gu, C., Chen, X. and Xu, B., (2021). "A discrete-continuum coupled numerical

method for fracturing behavior in concrete dams considering material heterogeneity", *Construction and Building Materials*, 305(1), 124741, https://doi.org/https://doi.org/10.1016/j.conbuildmat.2021.124741.

Rayleigh, J.W.S. and Lindsay, R.B., (1945). The theory of sound, Dover Publications.

Rots, J.G., Blaauwendraad, J., (1989). "Crack models for concrete, discrete or smeared? Fixed, multi-directional or rotating?", HERON, 34(1), 1-56.

Sinaie, S., Ngo, T.D. and Nguyen, V.P., (2018). "A discrete element model of concrete for cyclic loading", *Computers & Structures*, 196(1), 173-185, https://doi.org/https://doi.org/10.1016/j.compstruc.2017.11.014.

Valliappan, S., Yazdchi, M. and Khalili, N. (1999). "Seismic analysis of arch dams, A continuum damage mechanics approach", *International Journal for Numerical Methods in Engineering*, 45(11), 1695-1724, https://doi.org/10.1002/(SICI)1097-0207(19990820)45:11%3C1695::AID-NME651%3E3.0.CO;2-2.

Valliappan, S., Yazdchi, M. and Khalili, N., (1996). "Earthquake analysis of gravity dams based on damage mechanics concept", *International journal for numerical and analytical methods in geomechanics*, 20(10), 725-751, https://doi.org/10.1002/(SICI)1096-9853(199610)20:10%3C725::AID-NAG843%3E3.0.CO;2-X.

Voyiadjis, G.Z., Ahmed, B. and Park, T. (2021). "A review of continuum damage and plasticity in concrete, Part II: Numerical framework", *International Journal of Damage Mechanics*, 31(5), 762-794, https://doi.org/10.1177/10567895211063227.

Voyiadjis, G.Z. and Kattan, P.I. (2017). "A theory of damage and self-regenerating materials", *Acta Mechanica*, 228(12), 4249-4268, https://doi.org/10.1007/s00707-017-1928-y.

Wikipedia Contributors. (2022). Morrow Point Dam, (accessed 2.18.2022), https://en.wikipedia.org/w/index.php?title=Morrow_Point_Dam&oldid=1071488832.

Xu, L., Jing, S., Liu, J. and Huang, Y. (2017). "Cracking behavior of a concrete arch dam with weak upper abutment", *Mathematical Problems in Engineering*, 2017, 6541975, https://doi.org/10.1155/2017/6541975.